Received 2 August 2025; Accepted 11 December 2025
https://doi.org/10.48612/letters/2026-1-57-63
https://elibrary.ru/dxkbfu

Study of the density of states and optical absorption profile for PbS quantum dots with Cl and Fa ligands

N. V. Ermilov†, N. N. Bikkulova, A. R. Kurbangulov, G. R. Akmanova

†mr.nikolai.ermilov@ya.ru

Ufa University of Science and Technology, Ufa 450076, Russia

Abstract: Experimental studies of chalcogenides show that the higher mobility of Cl- and FA-liganded PbS quantum dots may be useful for efficient solar cell applications. However, a theoretical understanding of this mechanism is still lacking. This paper presents the results of modeling the electronic and optical structure as well as the carrier mobility of an array of Cl- and FA-liganded PbS quantum dots at different temperatures using the density functional theory in combination with the nonequilibrium Green's function method and the Landauer molecular dynamics approach. No signs of the formation of intermediate bands were found for the band structure of the quantum dot array with FA ligands. Instead, a continuum of bands with a lower band boundary was formed at an energy of about 0.6 eV. To better understand this phenomenon, the density of states and the optical absorption profile of PbS quantum dots with Cl and FA ligands were studied. It is found that FA-liganded quantum dots have higher mobility and improved optical absorption compared to Cl-liganded quantum dots. The differences can be explained by the features in the intermediate electronic structure.

Keywords: density of states, optical absorption profile, quantum dots, intermediate band, lead sulfide, ligands, formamidinium, electron conduction band

1. Introduction

Chalcogenides are binary chemical compounds of chalcogens (elements of the sixteenth group of the periodic table, which include oxygen, sulfur, selenium, tellurium, polonium and livermorium) with metals. Lead sulfide PbS are semiconductor materials used as IR detectors operating in the spectral range from 1 to 5 μm and in IR solar cells [1]. Good thermoelectric material is known to have a high value of dimensionless figure-of-merit (ZT). A significant amount of research has been devoted to studying ways to improve the thermoelectric properties of chalcogenides and their practical use.

Suyao Liu et al. showed that a step-by-step approach — lattice flattening, doping, and band engineering — allows for the optimal p-type PbS with $ZT \approx 1.0$ at 823 K. A crystal grown using the temperature gradient method achieves a record-breaking $ZT > 0.4$ at room temperature. Based on this material, a p-PbS/n-$Bi_2(Te,Se)_3$ cooling module was created, providing $\Delta T_{max} \approx 52$ K at $T_{hot} = 343$ K [3].

Zhongzhen Luo et al. explored midstates and nanoscale deposits using Ga doping and GeTe doping to significantly improve the performance of n-type PbTe. GeTe doping significantly increases the energy band gap of PbTe, and subsequent Ga doping introduces special midstates that lead to increased density of states (DOS), effective mass, and enhanced Seebeck coefficients. Moreover, nanoscale deposits of Ga_2Te_3 core and off-center dissonant Ge atoms in the PbTe matrix cause intense phonon scattering, greatly reducing the thermal conductivity (≈0.65 W/(m·K) at 623 K). As a result, high room temperature thermoelectric power $ZT \approx 0.59$ and peak $ZT_{max} \approx 1.47$ at 673 K were obtained for $Pb_{0.98}Ga_{0.02}Te$-5%GeTe. The average ZT value, which is most relevant for devices, is ≈1.27 from 400 to 773 K, the highest reported value for n-type PbTe [4].

Yan Zhong et al. achieved a significant improvement in the thermoelectric performance of p-type PbTe compared to its n-type counterpart, which still exhibited much lower thermoelectric performance. In doing so, not only effective mass engineering, resonant states, point defects, and nanostructures were summarized, but also newly developed concepts including dynamic doping to stabilize the optimal carrier concentration and dislocation introduction to reduce the lattice thermal conductivity were also presented. In addition, synergistic effects for further enhancing the thermoelectric performance have been outlined, as well as a discussion and prospects for accelerating the progress of n-type PbTe thermoelectric materials [5].

Shixuan Liu et al. reported ultra-high thermoelectric coefficient in as-cast n-type ingots with 0.3% copper addition in $PbTe_{0.9}PbS_{0.1}$ compound. The transmission electron microscopy (TEM) characterization showed that excess PbS was present in the PbTe matrix as strained endotaxial nanoprecipitates, which selectively affected the electrical and thermal conductivities: 1) the coherent PbTe/PbS lattice minimized the carrier scattering at the interface; 2) the periodic strain centers at the PbTe/PbS interface exhibited intense strain contrast, which could strongly scatter heat-carrying phonons. Electron backscatter diffraction (EBSD) characterization illustrated the very large PbTe grains (≈1 mm) in these as-cast ingots, resulting in extremely low

grain boundary scattering rates and hence very high charge carrier mobility. Ultimately, the $PbTe_{0.9}PbS_{0.1}$ + 0.3%Cu sample simultaneously achieved surprisingly high ZT_{max} values of ≈1.5 at 773 K and outstanding ZT values of ≈1.0 between 323 and 773 K; these values are highly competitive with those reported for state-of-the-art n-type PbTe materials [6].

Wei Wu et al. synthesized and characterized n-type $Pb_{0.97}Sb_{0.03}Te$ composites incorporating $Cu_{12}Sb_4S_{13}$ nanoparticles. Sb doping was used to change its carrier concentration to obtain n-type PbTe materials with high power factor. The introduction of $Cu_{12}Sb_4S_{13}$ nanoparticles generated a semi-coherent nanophase structure and simultaneously optimized the thermal and electrical properties due to remarkable energy filtering and interfacial scattering effects in the higher temperature range. Finally, the peak figure of merit ZT ≈1.58 was obtained at 773 K for the $Pb_{0.97}Sb_{0.03}Te$ + 1.5 wt.% $Cu_{12}Sb_4S_{13}$ sample, indicating that the incorporation of $Cu_{12}Sb_4S_{13}$ into $Pb_{0.97}Sb_{0.03}Te$ is an effective approach to improve its thermoelectric performance [7].

Min Liu et al. focused on and screened 12 potential metal electrodes in PbTe diffusion couples, confirming the superiority of Co as an electrode due to its low diffusion coefficient and interfacial resistance, inertia with respect to PbTe, and compatibility with sintering temperature. The strategy used in this work is also applicable to the selection of electrodes for other thermoelectric materials.

Increasing the efficiency of energy extraction from sunlight photons is one of the possible ways in the search for environmentally friendly energy. Solar cells based on quantum dots with ligands have been studied for use in new-generation photovoltaic devices [8, 9]. Optoelectronic materials based on chalcogenides with an intermediate absorption band have a significant impact on the efficiency of photovoltaic devices [10–14].

Due to the complexity of synthesis and characterization, a detailed experimental evaluation of the functional properties of these materials is time-consuming and expensive.

High-performance computing, which is a method of processing large amounts of data using powerful computers and storage devices combined into a single system, is an alternative method for studying the capabilities of thermoelectric compounds.

Using this method, it was possible to analyze the electronic properties of PbS quantum dots with Cl and FA ligands. No signs of an intermediate band were found for the band structure of the array of quantum dots with FA ligands. Instead, a continuum of bands was formed with a lower band boundary at an energy of about ≈0.6 eV [15].

The purpose of this work is to study the effect of Cl and FA ligands on the thermoelectric properties of PbS.

The obtained results of calculations of the energy band structure and the electron density distribution serve as a guideline for further research in the field of improving the efficiency of chalcogenide-based solar cells with ligand quantum dots.

2. Materials and methods

Ligands in this study can be defined as ions or molecules that donate their electron pair to another ion or atom (called the central atom) to form a coordination bond in a coordination compound. Thus, ligands act as electron donors and can be called Lewis bases. A ligand can be an anion, a cation, or a neutral chemical.

Cl^- (chloride ion) is a negatively charged species (anion) and belongs to the monodentate type of ligands in complex compounds. It has four electron pairs. It can donate only one electron pair to a single metal ion.

FA^+ (formamidinium) is a singly charged cation that is a component of halide perovskites. It can react with a metal halide to form a light-absorbing semiconductor material in perovskite solar cells. Also, formamidinium cations can partially or completely replace methylammonium halides in the formation of perovskite absorber layers in photovoltaic devices.

The density of states and the optical absorption coefficient were calculated using the density functional theory and linear combination of atomic orbitals (DFT-LCAO) method built into the Quantum ATK software [16].

The DFT method is that the energy of the electron system is uniquely determined by the electron density, without searching for a wave function. The electron density of the system is determined, which depends on three spatial coordinates, and a functional is found that relates the electron density to the energy of the system [17].

The LCAO method is that the valence electrons of the crystal are formed from atomic orbitals. A linear combination is made up of them. The movement of valence electrons is described by the Schrödinger equation, which is reduced to a system of linear equations for the coefficients [18].

The geometry of the liganded QDs is optimized through Quantum ATK software. In Quantum ATK software, global structural optimization is implemented through a genetic algorithm. It works by generating an initial set of random configurations and then evolving them using genetic operators.

The geometries of the QDs for both FA ligand and Cl ligand are optimized with DFT-LCAO method from a randomized initial structure.

In Quantum ATK, optical absorption is calculated within the linear-response framework based on DFT. After obtaining the electronic structure (band energies and eigenstates), the software computes the dipole transition matrix elements between occupied and unoccupied states and, on this basis, constructs the frequency-dependent dielectric function $\varepsilon(\omega)$ within the Independent-Particle Approximation. From the dielectric function, the following optical quantities are then derived:

– the absorption coefficient $\alpha(\omega)$,
– the refractive index $n(\omega)$,
– and the extinction coefficient $\kappa(\omega)$ [19].

The QDs are arranged on a square lattice of unit cell (1×1) with periodic boundary. The distances between QDs are set as 1.7 nm, which has been verified as the maximum distance that shows a coupling effect between QDs in the band structure.

The electronic and optical properties of PbS QD arrays without ligand, with FA ligand, and with Cl ligand are studied and compared. 10 ligands are added to one QD for both FA and Cl cases.

The temperature-dependent mobility of PbS quantum dots with organic Cl and FA ligands was calculated using Quantum ATK software. Molecular dynamics (MD) simulations with a nonequilibrium Green's function for quantum transport are provided by the so-called Landauer method [20 – 22].

Electron-phonon interaction plays an important role in the operation of most electronic devices. However, modeling this interaction is a challenging task for approaches based on the first Boltzmann transport equation [23 – 24].

One of the most serious drawbacks of these approaches, such as the electron-phonon interaction in the Boltzmann equation and the nonequilibrium Green's function method, is the harmonic approximation for phonons, since the introduction of anharmonic effects significantly increases the computational cost. But for most materials at room temperature and above, the anharmonic contribution to phonons is significant, so it is difficult to properly account for it using these approaches [25].

In this study, the electron-phonon interaction was taken into account using MD simulations, and the charge carrier transport properties were calculated using the DFT nonequilibrium Green's function (NEGF) method and the Landauer formula.

This approach involves simulating the operation of the device with fixed left and right electrodes. The central charge transport region was subjected to MD simulations at different temperatures and corresponding nonequilibrium Green's functions to determine the conductivity $G(l, T)$ based on the transmittance $J(E, T)$. Figure 1 shows the operating principle of the proposed modeling method.

For the given MD-region length and temperature T, an equilibrium lattice is first generated, and the transmission $J(E, T)$ is then computed using the DFT-NEGF method, averaged over MD configurations. Using the Landauer formula, electrical conductivity and resistance are extracted. This procedure is repeated for several MD-region lengths (l_0, l_3, l_4, l_5), corresponding to 0, 3, 4, and 5 doped quantum dots between the electrodes. The dependence of resistance on length is then used to obtain $\rho_1 D(T)$ via linear least-squares fitting [26].

3. Results

The density of states, optical absorption, and orbital-projected density of states for Cl- and FA-liganded PbS quantum dots were investigated. Figures 2 – 7 show the calculated values of the density of states and orbital-projected optical absorption for FA-liganded and Cl-liganded quantum dots.

The obtained density of states simulation data shows a distinct peak in the conduction band near the Fermi level for the Cl-liganded quantum dots (highlighted by the red dotted line in Fig. 5). This peak is absent in the density of states for the FA-liganded quantum dots (Fig. 2), and the density of states for the FA-liganded quantum dots in the conduction band is generally higher. The difference in the density of states may affect the optical properties of the quantum dots, which is supported by the optical absorption data (Fig. 3 and Fig. 6). The optical absorption coefficient of the Cl-liganded quantum dots also shows an isolated peak at about 1.5 eV (highlighted by the red dotted line in Fig. 6), but this peak is not observed in the data for the FA-liganded quantum dots. The difference can be explained by comparing the orbital projections of the density of states (Fig. 4 and Fig. 7). The spectrum of 2p orbitals of quantum dots with the FA ligand has one additional peak in the energy range of 0.6 – 2.0 eV in the conduction band, while for the Cl ligand such a peak

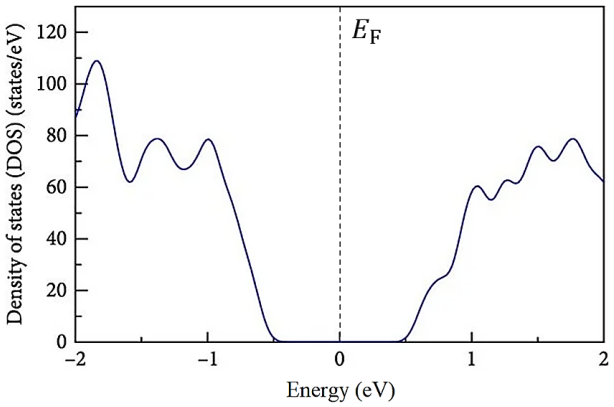

Fig. 2. Density of states of PbS quantum dots with FA ligands.

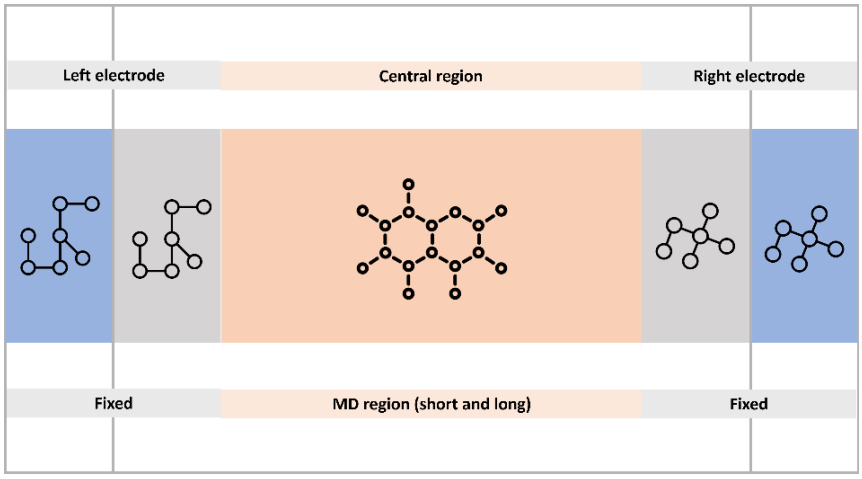

Fig. 1. (Color online) Schematic diagram of the modeling of the dependence of mobility on temperature using the Landauer method.

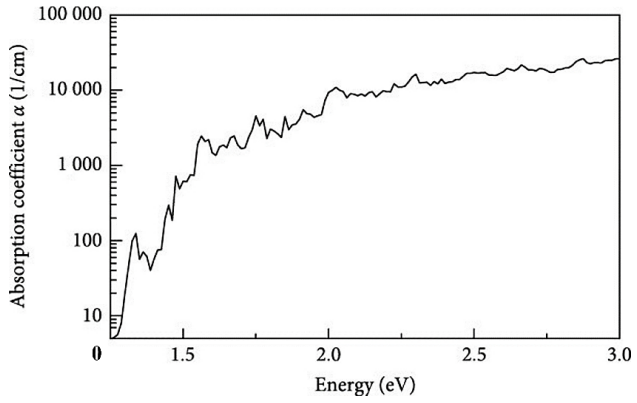

Fig. 3. Optical absorption of PbS quantum dots with FA ligands.

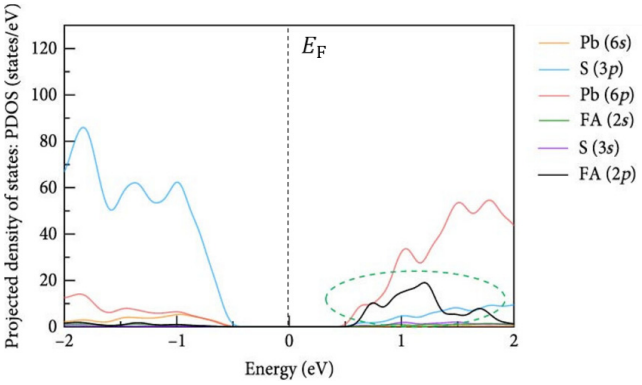

Fig. 4. (Color online) Orbital-projected density of states for PbS quantum dots with FA ligands. The effect of p-orbital density of states hybridization (black solid line) in the conduction band is highlighted by the green dotted line.

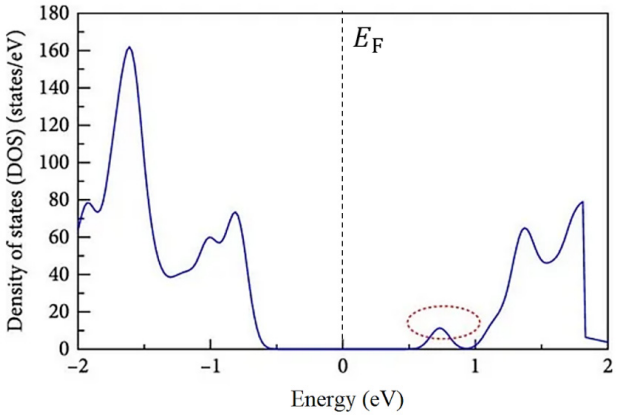

Fig. 5. (Color online) Density of states of PbS quantum dots with Cl ligands. The contribution of the intermediate band is highlighted by the red dotted circle.

is absent. Hybridization of the 2*p* orbital with other orbitals may be the reason for the absence of an intermediate band for quantum dots with the FA ligand. This refers to the hybridization of 2*p* orbitals with *d* orbitals of transition metal atoms, which forms *p*-*d* bonding states.

Gaussian broadening with a parameter $\sigma = 0.05$ eV (corresponding to a half-width at half-maximum of ≈0.12 eV) was used to calculate the absorption spectra of PbS quantum dots with FA and Cl ligands.

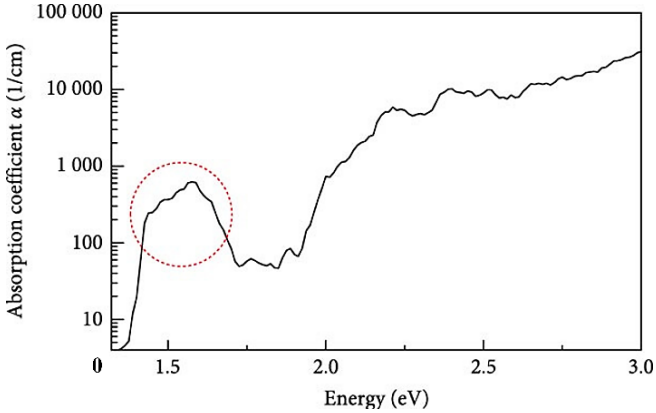

Fig. 6. Optical absorption of PbS quantum dots with Cl-ligands. The contribution of the intermediate band is highlighted by the red dotted line.

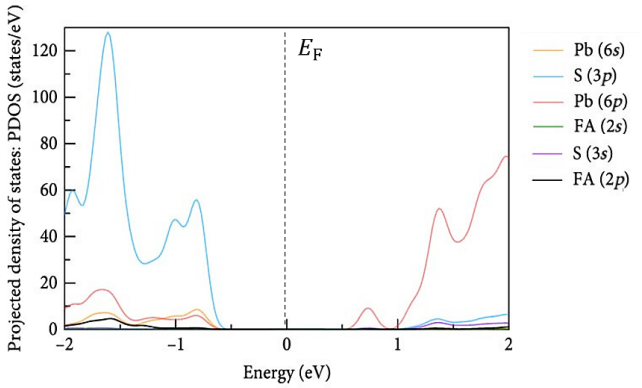

Fig. 7. (Color online) Orbital-projected density of states of quantum dots with Cl ligands. The density of states of the p orbitals (black solid line) does not show the effect of hybridization in the conduction band.

To understand how charge carriers move in the quantum dot arrays, the mobility of the quantum dot array junctions is calculated over a wide temperature range using the Landauer molecular dynamics method.

Figure 1 shows the junction structure with elements of the left and right electrodes as well as the central molecular dynamics region. The one-dimensional quantum dot array is sandwiched between two $CH(NH_2)_2PbI_3$ electrodes.

During the calculations, the quantum dot arrays were connected with different numbers of quantum dots and different lengths of the quantum dot arrays. One-dimensional PbS quantum dot arrays are the middle domain for the MD-Landauer calculations.

Figures 8 and 9 show the simulation and regression results for quantum dots with FA and Cl ligands, respectively, at 300 K. Figure 10 shows the log-linear mobility plot. Figure 10 clearly shows that quantum dots with FA ligand (red solid line with round marker) have higher mobility than quantum dots with Cl ligand (blue solid line with square marker) at room temperature. For quantum dots with FA ligand at 300 K, the resistivity $\rho_{bulk} = 102\,000$ Ω·m was obtained by linearly fitting the data as shown in The mobility was calculated as $\mu = 0.001394$ $cm^2 \cdot V^{-1} \cdot s^{-1}$, where the carrier density $n = 4.39 \cdot 10^{14}$ cm^{-3} was used. The carrier concentration value was obtained using DFT calculations. The concentration was determined by integrating the density of states above the

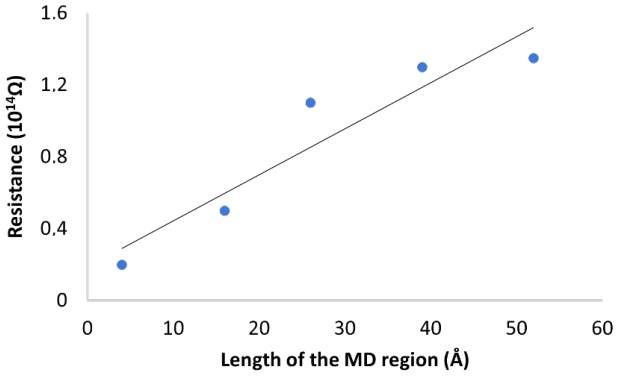

Fig. 8. (Color online) Resistance versus length of the MD region for a junction with an FA-liganded quantum dot array. The *y* scale is in 10^{14} Ω. A linear regression (black solid line) is performed to extract the resistivity ρ_{bulk} = 102 000 Ω·m. The temperature is 300 K.

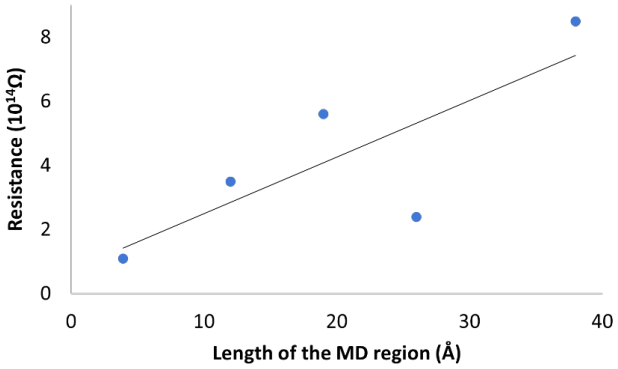

Fig. 9. (Color online) Resistance versus length of the MD region for a junction with an Cl-liganded quantum dot array. The *y* scale is in 10^{14} Ω. A linear regression (black solid line) is performed to extract the resistivity ρ_{bulk} = 748 000 Ω·m. The temperature is 300 K.

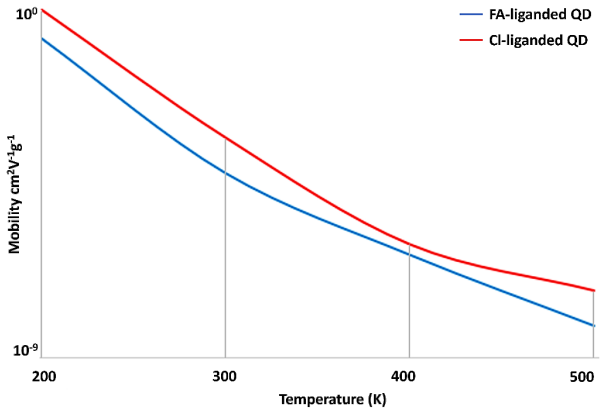

Fig. 10. (Color online)Logarithmic linear plot of mobility versus temperature. FA-liganded quantum dots (red solid line) have higher mobility than Cl-liganded quantum dots (blue solid line) near room temperature.

Fermi level, taking account for the Fermi-Dirac distribution at the operating temperature and the volume of the simulated cell. For quantum dots with Cl ligands at 300 K, the resistivity is ρ_{bulk} = 748 000 Ω·m using the data as shown in Fig. 9, and the mobility is μ = 0.0001481 $cm^2 \cdot V^{-1} \cdot s^{-1}$ using the carrier density $n = 5.635 \cdot 10^{14}$ cm^{-3}. The values of the carrier concentration are obtained from electronic structure calculations based on the density of states and the position of the Fermi level at a given temperature.

According to the simulation data, the mobility of the FA and Cl liganded QD arrays decreases with increasing temperature. Similar behavior as a function of temperature was observed in the simulation of bulk silicon and silicon nanowire mobility using the same approach [26]. It was found that FA liganded PbS QD arrays generally have higher mobility than Cl liganded QD arrays over a wide temperature range.

The increased mobility observed in FA liganded PbS QDs can be explained by the absence of the intermediate band in FA liganded QD arrays.

This fact also influences the optical absorption data, where the FA-liganded quantum dots have a bulk-like absorption profile, without an isolated peak and with a higher optical absorption value than the Cl-liganded quantum dots. The density of states data indicates that the disappearance of discrete features in the FA-liganded sample may be due to hybridization of the 2*p* orbitals with other orbitals.

The simulations show that the mobility in the FA and Cl-liganded CT matrices decreases with increasing temperature. A similar temperature dependence was previously observed for bulk silicon and silicon nanowires using the same method. However, the FA-liganded PbS CT matrices exhibit generally higher mobility compared to the Cl-liganded matrices over a wide temperature range [27].

4. Discussion

After examining the simulated charge carrier density for the PbS quantum dot array with FA and Cl ligands, it was found that the charge carrier density of the FA ligand sample is much smaller than that of the Cl ligand sample. The band gap value of the FA ligand sample is the smallest compared with those of the unliganded PbS quantum dot array and the Cl ligand quantum dot array. It would be expected that the charge carrier density of the FA ligand sample would be higher due to the narrower band gap. Figure 2 shows that the gap for FA is 1 eV, in Fig. 5 it can be seen that for Cl it is approximately 1.2 eV. For comparison, we took separate calculations for pure PbS. The band gap value obtained by other authors is ≈0.41 eV [28].

However, the simulated charge carrier density obtained from careful analysis of the DFT simulation results showed the opposite trend. This effect can be explained by the presence of multiple energy bands in both the ligand-free and Cl-liganded PbS quantum dot array samples. The additional intermediate band provides an additional channel for charge carrier generation, which is an attractive feature of intermediate band solar cells [29].

However, as follows from mobility modeling, the increased carrier density will inevitably lead to decreased mobility, which is the main obstacle that has been shown experimentally and theoretically to prevent the creation of highly efficient intermediate band solar cells [30 – 31].

When optimizing the energy yield of photovoltaic devices, both charge carrier transport and optical properties must be considered.

5. Conclusions

In this study, we analyzed the results of density of states and optical absorption profile calculations of Cl- and FA-liganded PbS quantum dots after the absence of signs of intermediate band formation was previously found for the band structure of FA-liganded quantum dot arrays.

The difference in the density of states may affect the optical properties of quantum dots, which is confirmed by the optical absorption data. Hybridization of the 2*p* orbital with other orbitals may be the reason for the absence of an intermediate band for FA-liganded quantum dots. FA-liganded PbS quantum dots showed higher optical absorption coefficients due to the elimination of intermediate levels or bands, which in turn indicates a difference in the transport properties of Cl- and FA-liganded PbS.

To test the above hypothesis, we simulated and compared the mobility of PbS quantum dot arrays with Cl and FA ligands over a wide temperature range. During the simulation, it was found that the mobility of charge carriers in quantum dots with FA ligands is higher than in quantum dots with Cl ligands over a wide temperature range. In addition, calculations of the electronic structure and optical absorption show that the presence or absence of an intermediate band plays an important role in changing the transport properties. The intermediate band provides an additional relaxation channel due to scattering and, therefore, can hinder the transfer of charge carriers.

The results of the simulation confirm this hypothesis and serve as a guide for further research in the field of increasing the efficiency of solar cells based on chalcogenides with liganded quantum dots. The calculations performed in this study provide fundamental guidance for more efficient solar cell design.

References

1. A. Rogalski, History of infrared detectors, Opto-Electronics Review 20 (2012) 279 – 308.
2. R. J. Korkosz, T. C. Chasapis, S. H. Lo, J. W. Doak High *ZT* in p-type $(PbTe)_{1-2x}(PbSe)_x(PbS)_x$ thermoelectric materials. Journal of the American Chemical Society 136 (8) (2012) 3225 – 3227.
3. L. Suyao, B. Shulin, G. Tian Promoting p-Type PbS as Efficient Candidates for Thermoelectric Cooling and Power Generation. Wiley. Advanced Functional Materials (2025) e16306.
4. Z. Luo, S. Cai, S. Hao, T. Bailey, Strong Valence Band Convergence to Enhance Thermoelectric Performance in PbSe with Two Chemically Independent Controls. Angew Chem Int Ed Engl. 60 (1) (2021) 268 – 273.
5. M. Zhang, J. Cai, F. Gao, Z. Zhang, M. Li, Z. Chen, Y. Wang, D. Hu, X. Tan, G. Liu, S. Yue, J. Jiang, Improved Thermoelectric Performance of p-Type PbTe by Entropy Engineering and Temperature-Dependent Precipitates, ACS Appl. Mater. Interfaces 16 (2024) 907 – 914.
6. S. Liu, Y. Yu, D. Wu, X. Xu, X. Chao, Z. Yang, J. He, Strained Endotaxial PbS Nanoprecipitates Boosting Ultrahigh Thermoelectric Quality Factor in n-Type PbTe As-Cast Ingots, Small 17 (2021) 2104496.
7. W. Wu, C. Zhu, H. Ming, T. Chen, D. Li Achieving higher thermoelectric performance of n-type PbTe by adjusting the band structure and enhanced phonon scattering. Nanoscale 14 (46) (2022) 17163 –17169.
8. S. Ding, M. Hao, T. Lin, Y. Bai, L. Wang, Ligand engineering of perovskite quantum dots for efficient and stable solar cells, Journal of Energy Chemistry 69 (2022) 626 – 648.
9. M. Hao, Y. Bai, S. Zeiske, L. Ren, J. Liu, Y. Yuan, N. Zarrabi, N. Cheng, M. Ghasemi, P. Chen, M. Lyu, D. He, J.-H. Yun, Y. Du, Y. Wang, S. Ding, A. Armin, P. Meredith, G. Liu, H.-M. Cheng, L. Wang, Ligand-assisted cation-exchange engineering for high-efficiency colloidal $Cs_{1-x}FA_xPbI_3$ quantum dot solar cells with reduced phase segregation, Nat. Energy 5 (2020) 79 – 88.
10. A. Luque, A. Martí, Increasing the Efficiency of Ideal Solar Cells by Photon Induced Transitions at Intermediate Levels, Phys. Rev. Lett. 78 (1997) 5014 – 5017.
11. Y. Okada, T. Sogabe, A. J. Nozik, G. Conibeer, Intermediate band solar cells, Energy and Environment Series, 2014, Royal Society of Chemistry, Cambridge, 425 – 454.
12. H. Li, Q. Wang, Y. Oteki, C. Ding, D. Liu, Y. Guo, Y. Li, Y. Wei, D. Wang, Y. Yang, T. Masuda, M. Chen, Z. Zhang, T. Sogabe, S. Hayase, Y. Okada, S. Iikubo, Q. Shen, Enhanced Hot-Phonon Bottleneck Effect on Slowing Hot Carrier Cooling in Metal Halide Perovskite Quantum Dots with Alloyed A-Site, Advanced Materials 35 (2023) 2301834.
13. I. Ramiro, A. Marti, E. Antolin, Review of experimental results related to the operation of intermediate band solar cells, IEEE Journal of Photovoltaics 4 (2) (2014) 736 – 748.
14. C. Gayner, K. K. Kar, Recent advances in thermoelectric materials, Progress in Materials Science 83 (2016) 330 – 382.
15. N. V. Ermilov, N. N. Bikkulova, A. R. Kurbangulov, G. R. Akmanova, I. M. Munasypov, Study of band structures of PbS quantum dots with Cl and Fa ligands, Engineering Physics 2 (2025) 3 – 9. (in Russian)
16. J. C. Reinstra-Kiracofe, G. S. Tschumper, G. F. Schaefer III, S. Nandi, G. B. Ellison, Electrical properties of lead, Chem. Rev. 102 (2002) 231 – 282.
17. A. Pimachev, Y. Dahnovsky, Optical and magnetic properties of PbS nanocrystals doped by manganese impurities, The Journal of Physical Chemistry C 119 (29) (2015) 16941 – 16946.
18. R. Landauer, Spatial variation of currents and fields due to localized scatterers in metallic conduction, IBM Journal of Research and Development 1 (3) (1957) 223 – 231.
19. QuantumATK Reference Manual. OpticalSpectrum. QuantumATK Available online
20. L. P. Kadanoff, G. Baym, Quantum Statistical Mechanics: Green's Function Methods in Equilibrium and Nonequilibrium Problems, 1st ed., CRC Press, 2018.
21. T. Markussen, M. Palsgaard, D. Stradi, T. Gunst, M. Brandbyge, K. Stokbro, Electron-phonon scattering from Green's function transport combined with molecular dynamics: Applications to mobility predictions, Phys. Rev. B 95 (2017) 245210.
22. R. Rhyner, M. Luisier, Atomistic modeling of coupled

electron-phonon transport in nanowire transistors, Phys. Rev. B 89 (2014) 235311.
23. C.-H. Park, N. Bonini, T. Sohier, G. Samsonidze, B. Kozinsky, M. Calandra, F. Mauri, N. Marzari, Electron — Phonon Interactions and the Intrinsic Electrical Resistivity of Graphene, Nano Lett. 14 (2014) 1113–1119.
24. K. Kaasbjerg, K. S. Thygesen, K. W. Jacobsen, Unraveling the acoustic electron-phonon interaction in graphene, Phys. Rev. B 85 (2012) 165440.
25. M.-H. Cha, J. Hwang, Quantum transport in a chain of quantum dots with inhomogeneous size distribution and manifestation of 1D Anderson localization, Sci Rep 10 (2020) 16701.
26. K. Kumakura, C. Chen, T. Sogab, Electronic-, Optical-, and Temperature-Dependent Carrier Mobility Simulations of Perovskite-Type Liganded PbS Quantum Dot Array, Condensed Matter Physics 2023 (2023) 1–10.
27. T. Markussen, M. Palsgaard, D. Stradi, T. Gunst, M. Brandbyge, Electron-phonon scattering from Green's function transport combined with molecular dynamics: Applications to mobility predictions, Phys. Rev. B 95 (2017) 245210.
28. O. Madelung, Semiconductors: Data Handbook, Springer, 2004.
29. G. Madsen, D. Singh, BoltzTraP. A code for calculating band-structure dependent quantities, Comput. Phys. Commun. 175 (2006) 67.
30. T. Sogabe, Y. Shoji, M. Ohba, K. Yoshida, R. Tamaki, H.-F. Hong, C.-H. Wu, C.-T. Kuo, S. Tomić, Y. Okada, Intermediate-band dynamics of quantum dots solar cell in concentrator photovoltaic modules, Sci. Rep. 4 (2014) 4792.
31. Y. Okada, N. J. Ekins-Daukes, T. Kita, R. Tamaki, M. Yoshida, A. Pusch, O. Hess, C. C. Phillips, D. J. Farrell, K. Yoshida, N. Ahsan, Y. Shoji, T. Sogabe, J.-F. Guillemoles, Intermediate band solar cells: Recent progress and future directions, Applied Physics Reviews 2 (2015) 021302.